Characterization of sub-picosecond laser-produced fast electrons by modeling angularly resolved bremsstrahlung measurements with 3-D hybrid particle-in-cell code

L. Chen[1)*] and H. Sawada[2)]
Department of Physics, University of Nevada Reno, Reno, NV, 89557, USA
1) leichen@unr.edu, 2) hsawada@unr.edu
* corresponding author

ABSTRACT
Hard x-rays produced by intense laser-produced fast electrons interacting with solids are a vital source for producing radiographs of high-density objects and implosion cores for inertial confinement fusion. Accurate calculation of hard x-ray sources requires a 3-D simulation geometry that fully models the electron transport dynamics, including electron recirculation and the generation of absolute photon yields. To date, 3-D simulations of laser-produced bremsstrahlung photons over tens of picoseconds and code benchmarking have not been performed definitively. In this study, we characterize sub-picosecond laser-produced fast electrons by modeling angularly resolved bremsstrahlung measurements for refluxing and non-refluxing targets using the 3-D hybrid particle-in-cell (PIC), Large Scale Plasma (LSP) code. Bremsstrahlung radiation and escaped electron data were obtained by focusing a 50-TW Leopard laser (15J, 0.35 ps, 2×10^{19} W/cm^2) on a 100-μm-thick Cu foil and a Cu with a large plastic backing (Cu-CH target). Data for both the Cu and Cu-CH targets were reproduced for simulations with a given set of electron parameters. Comparison of the simulations revealed that the hard x-ray emission from the Cu target was significantly longer in duration than that from the Cu-CH target. The benchmarked hybrid PIC code could prove to be a powerful tool in the design and optimization of time- and angular-dependent bremsstrahlung sources for flash x-ray and gamma-ray radiography.

1. Introduction

Interaction of a relativistic intense, short-pulse laser with a solid target generates energetic (fast) mega-electron volt (MeV) electrons, producing a broad spectrum of hard x-rays.[1,2] Understanding the characteristics of fast electrons is critical not only in the fields of hard x-ray radiography of mm-scale solid high-Z objects[3,4] and inertial confinement fusion (ICF) implosion cores,[5,6,7] but also for applications using fast electrons such as the fast ignition ICF,[8,9] creation of warm dense matter (WDM)[10] and the generation of secondary sources including MeV bremsstrahlung[11,12,13]. In particular, information on the electron energy distribution (T_h), the laser-to-electron energy conversion efficiency (η), and the electron beam divergence angle (θ)[14,15] is important, forming the key initial conditions in calculations of space- and time-dependent x-ray photon generation.

Spectrally resolved bremsstrahlung measurements are commonly used to retrieve the fast electron characteristics in high-intensity short-pulse laser experiments among other x-ray and particle measurements.[16,17,18] A broad spectrum of x-ray photons up to ~MeV is recorded by spectrometers consisting of stacks of alternating differential metal filters and detector layers.[19,20,21,22] X-ray signals recorded in each detector layer are modeled with a Monte Carlo or a hybrid particle-in-cell (PIC) code by varying the input electron parameters until the simulation results match the experiment.[23,24,25,26,27,28,29] To further constrain the fitting of parameters, the angularly and spectrally resolved bremsstrahlung spectra have been measured by configuring multiple identical spectrometers around the target.[30,31,32,33,34,35,36] Despite a variety of such measurement strategies, comparisons of multiple bremsstrahlung signals with simulations using several different numerical approaches have provided limited consensus. This is partly attributed to the lack of a simulation dimension and/or time in modeling the electron recirculation (refluxing).[37,38,39] This phenomenon occurs when a strong sheath field generated at the target-vacuum boundaries traps and reflects escaping fast electrons back into the target. As a consequence, the electron trajectories are altered significantly, resulting in changes in the angular distribution of the bremsstrahlung radiation. Modeling of electron transport including electron recirculation requires a three-dimensional simulation with sufficiently large vacuum spaces and a long simulation time to calculate the self-generated electromagnetic fields and collisional energy losses during the electron recirculation.

Here, fast electron characterization is revealed by modeling the angularly resolved bremsstrahlung measurements for both refluxing and non-refluxing targets with a 3-D hybrid PIC Large Scale Plasma (LSP) code.[40] The bremsstrahlung and the escaped electron data were obtained from a 100-μm-thick Cu foil and also for a Cu foil attached to a large plastic backing[41,42,43] (Cu-CH target) to minimize electron recirculation. It was found that simultaneous fitting to the two measured bremsstrahlung signals for both the Cu and Cu-CH targets were necessary to determine all three electron parameters. Using the benchmarked code, the time evolution of the bremsstrahlung spectra for the Cu and Cu-CH targets were compared. The simulations which ran for up to 40 ps, revealed for the first time that the electron recirculation makes the duration of the hard x-ray emission

significantly longer in the Cu foil than in the Cu-CH target. The volume of the plastic backing necessary to eliminate the bremsstrahlung produced by the electron recirculation was also investigated numerically.

This paper is organized as follows: Section II describes the Leopard laser experiment used to obtain data for the code benchmarking. Section III describes the 3-D hybrid PIC simulations including the simulation setup, the field generation, the electron trajectory, and the synthetic angular-dependent bremsstrahlung. Section IV presents the results for the direct comparisons of measured and simulated signals and the chi-squared values of the fittings to the Cu-CH and Cu data. Numerical simulations of the time evolution of the bremsstrahlung and a discussion on the effect of the volume of plastic backing on bremsstrahlung generated by electron recirculation are presented in the final section.

II. Experiment

The experiment was conducted using the 50 TW Leopard laser [44] at the University of Nevada, Reno. A schematic of the experiment is given in Figure 1(a). The Leopard laser produced a pulse of energy of ~15 J with a pulse duration of 0.35 ps (full width at half maximum, FWHM) at a central wavelength of 1057 nm. The beam was focused tightly with an f/1.5 dielectric coated off-axis parabolic mirror onto the target at an incident angle of 30° with an S-polarization. Measurement of the beam energy in the target plane showed 30% of the laser energy was contained within an ~8 μm diameter spot.[45] The on-target peak laser intensity was estimated to be $\sim 2\times10^{19}$ W/cm^2. Bremsstrahlung photons generated during the electron transport were recorded using two calibrated differential filter stack spectrometers[20] at the positions of 22° and 40° from the laser axis. The spectral range covered by the spectrometers was from 10 to 800 keV. A magnet-based electron spectrometer[46] was used to measure the number of escaped electrons along the laser axis.

Two types of targets were used in the experiment: a 100-μm-thick Cu foil and a Cu foil attached to a polystyrene (CH) hemisphere post with a quarter-inch radius (6350 μm). The surface area of the Cu foil was 1 mm^2. The large CH piece allowed fast electrons to travel continuously from the Cu to the CH, and the electrons were prevented from recirculating back to the Cu foil for further x-ray generation. A low-Z backing material was chosen to minimize x-ray generation from the backing, thus making the Cu foil the dominant source of bremsstrahlung radiation.

Figure 1(b) shows the measured electron spectra for the Cu and Cu-CH targets. Both spectra fit well with a single exponential slope of 1.25 ± 0.15 MeV for the Cu and 1.15 ± 0.35 MeV for the Cu-CH target. Some of the high energy electrons (> ~3 MeV) deviated from the single slope spectrum, but their contribution to bremsstrahlung generation was minor as discussed later. At least two target shots for each laser and target condition were performed. The shot-to-shot variation in the slope temperature was less than 10%. The inferred slope temperatures were comparable for the two cases as expected given that any difference between them would arise whether the CH backing was used or not. The slope of the escaped electrons along the laser axis relates directly to that of the electrons generated near the laser interaction region.[47,48] The number of escaped electrons from the Cu foil was consistently higher than the number from the Cu-CH target. As reported,[49,50,51] the magnitude of the rear sheath field is proportional to the square root of the electron number. As the target becomes thicker, the number of electrons escaping from the rear of the target decreases due to the angular spread of the electron beam.

The measured bremsstrahlung signals at 22° (Brems1) and 40° (Brems2) for both targets are presented in Figures 1(c) and 1(d), respectively. The intensity of the bremsstrahlung decreased with the angular position of the spectrometer away from the laser axis (i.e., the signal was higher at 22° than at 40°). The CH post, which prevented electron recirculation, reduced the bremsstrahlung signals by a factor of 2 in the seventh layer (~50 keV) in both detectors. Later, the measured signals at the two spectrometer positions were compared directly and fitted simultaneously with simulations by varying the input divergence angles and the electron beam energies for the Cu-CH and Cu targets as discussed in Sections IV.A and IV B, respectively.

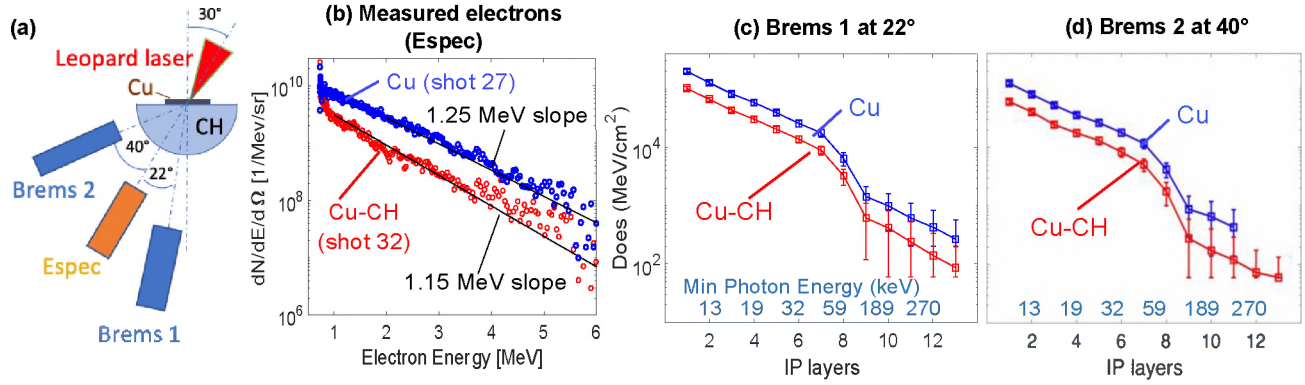

FIG. 1. (a) Schematic diagram of the experimental and diagnostic layout. (b) Measured escaped electron spectra for the bare Cu foil and the Cu-CH target. The measured bremsstrahlung spectrometer signals (doses) at (c) 22° and (d) 40° from the laser direction for the two types of targets.

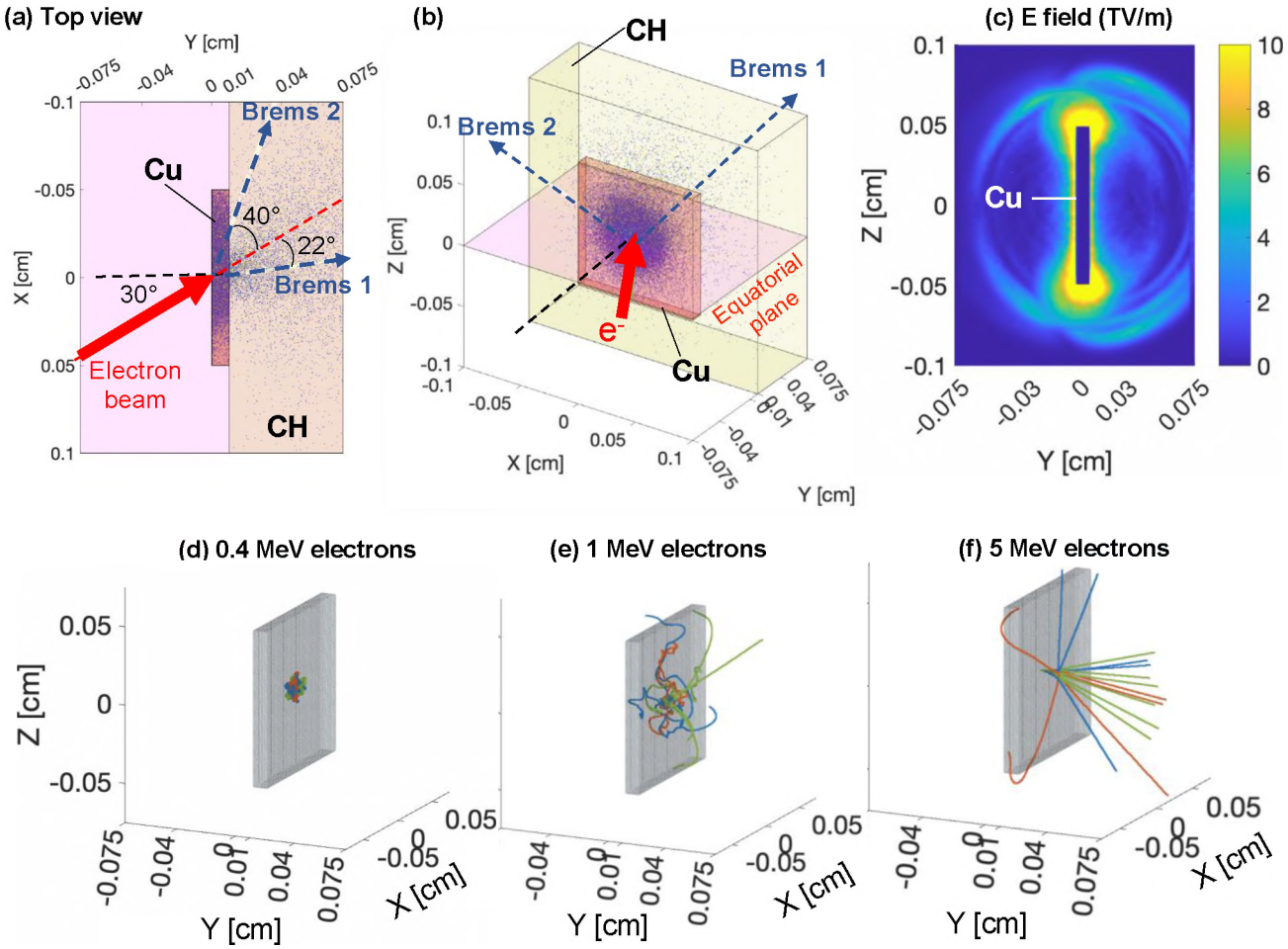

FIG. 2.3-D hybrid PIC LSP simulation setup for the Cu-CH target. (a) Top view and (b) 50° view from the equatorial plane. The injection axis of an electron beam and the diagnostics are both in the equatorial plane. Blue dots are fast electrons. (c) Map of the total electric fields in the Y-Z plane at X=0 μm. The trajectories for fast electrons (d) 0.4 MeV, (e) 1.0 MeV, and (f) 5 MeV electrons. Different colors represent particles injected at different times (1.0 ps in blue, 1.2 ps in orange and 1.4 ps in green).

III. 3-D LSP modeling of angularly resolved bremsstrahlung

Simulations of fast electron transport and hard x-ray generation were performed using a 3-D hybrid PIC LSP code. The simulations were initiated by injecting a beam of fast electrons, instead of solving a laser-target interaction. The use of 3-D cartesian coordinates was essential in this work to compute the development of self-consistent fields at all target-vacuum boundaries and to model the off-axis incident angle of an injected electron beam that mimics the laser incident angle with respect to the detector positions in the experiment. Magnetic fields generated by resistive gradients or filamentation are not included. The code takes into account the stopping power, scattering, and radiative loss for the electron transport processes. [52, 53] The generation of bremsstrahlung and Kα photons in the LSP is modeled using a cross-section calculated with the Integrated Tiger Series (ITS). [54] We benchmarked the LSP calculations of the electron stopping and scattering as well as the angular distribution of bremsstrahlung generated in solid Cu against the Monte Carlo code Electron Gamma Shower 5 (EGS5)[55] in the Particle and Heavy Ion Transport code System (PHITS).[56]

The simulation box size was large enough to calculate the development of electric and magnetic fields surrounding the Cu target. A 100-μm-thick Cu foil with a surface area of 1 mm^2 was positioned at the center of a 2×1.5×2 mm^3 simulation box with a cell size of 10 μm, resulting in ~ 500 μm vacuum spaces all around the Cu foil. For the Cu-CH target, a 650-μm-thick plastic layer with a 2×2 mm^2 surface area was attached to the rear side of the Cu. Given that absorbing boundaries were used, the plastic reaching the boundaries was essentially an infinitely large layer. The simulation setup and the electron beam injection axis for the Cu-CH target at an incident angle of 30° in the equatorial plane are illustrated in Figures 2(a) and 2(b). The duration of

the electron beam was assumed to be the same as that of the laser pulse (0.35 ps FWHM), and most simulations were run for 20 ps. The main electron source parameters varied for fitting were the divergence angle and electron beam energy as discussed later.

The major difference between the hybrid PIC code and the Monte Carlo code is self-consistent field generation associated with electron transport in the hybrid PIC simulations. The time evolution of the electric and magnetic fields as well as the trajectories of fast electrons with various energies were simulated using the parameters of T_h = 1.0 MeV, θ = 50°, and beam energy, E_b = 1.1 J. A snapshot of the total electric field in the Y-Z plane (X=0) at 4 ps is shown in Figure 2(c). The magnitude of the peak electric fields generated around the Cu foil exceeded 10 TV/m. The trajectories for 0.4, 1.0, and 5.0 MeV electrons for simulation times up to 5 ps are shown in Figures 2(d)-2(f). The 0.4-MeV electrons were stopped collisionally in the Cu foil. Most of the 1-MeV electrons were affected by the front and rear sheath fields, forcing the electrons to propagate to the edge of the foil. These electrons propagate on the target surface toward the foil edges rather than penetrate back into the target. As a result, strong sheath fields were also established near the Cu edges at Z=±0.05 cm as in Fig. 2(c). The majority of the 5-MeV electrons escaped from the rear of the target, and some of the electrons injected at the peak of the pulse (orange lines) were largely deflected and pulled back by the fields to the corner of the foil, as shown in Fig. 2(f). These simulations demonstrate that: (1) The non-normal electron injection produces an asymmetric electron beam distribution with respect to the target normal [Fig. 2(a)], affecting the resulting bremsstrahlung angular distribution to be also asymmetric. [e.g., compare the electron number density (blue dots) at the Brems2 position at 70° from the target normal in clockwise vs counterclockwise]. (2) Bremsstrahlung radiation generated from electron recirculation is dominated by electrons with energies less than ~5 MeV. (3) Electrons trapped by the rear sheath field are deflected sideways rather than forced to execute simple back-and-forth motion within the foil.

Photons generated in the Cu and CH layers were post-processed to compute the time- and angular-dependent photon spectra and the synthetic bremsstrahlung spectrometer doses using a spectrometer response function.[20] The time-integrated bremsstrahlung spectra and the spectrometer doses at the 22° (Brems1) and 40° (Brems2) detector positions for the Cu-CH target are presented in Figures 3(a) and 3(b). The electron parameters used for the simulation were T_h = 1 MeV, θ = 50°, and E_b = 1.5 J. The broadband x-ray spectrum consisted of bremsstrahlung radiation above ~10 keV and the characteristic Cu K-photons near 8 keV. The calculated x-ray spectrum in Fig. 3(a) was converted to simulated doses for each image plate (IP) layer of the spectrometer to directly compare them with the measurements in absolute units (next section). Both the raw x-ray spectra and the spectrometer doses showed higher signals at 22° (close to the electron injection axis) than at 40° for a T_h of ~1 MeV. The angular distribution of bremsstrahlung depends on the target material, the thickness of the target and the fast electron spectrum (or laser intensity). Here, the measured anisotropy of the bremsstrahlung signals was attributed to the 100-μm-thick Cu foil because such measurements are nearly isotropic with a T_h of ~0.6 MeV as in a previous experiment.[57] It is reported that the isotropic hard x-ray emission originates from thin foil or wire targets (< 10 μm) due to the strong electron recirculation even at a peak laser intensity of 10^{20} W/cm^2.[36]

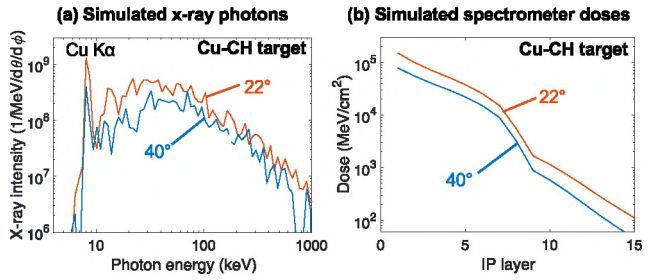

FIG. 3. (a) Calculated bremsstrahlung spectra at the 22° and 40° positions for the Cu-CH target. (b) Synthetic spectrometer doses as a function of the image plate (IP) layers after the spectra in (a) are processed using a detector response function.

IV. Results and discussions

A. Fitting to the bremsstrahlung measurements for the Cu-CH target

The measured bremsstrahlung doses were fitted with a series of LSP simulations by changing the electron beam energy, E_b, and the divergence angles, θ. The ranges of E_b and θ were varied between 0.5 and 2.0 J and 10° and 90°, respectively. For each spectrometer, the fitted residuals between the measured and simulated doses were calculated using the chi-squared method, in which the chi-squared value was examined by calculating $\chi^2 = \sum_{i=1}^{n} \frac{(y_{exp}-y_{sim})_i^2}{\sigma_i^2}$, where y_{exp} and y_{sim} were the measured and simulated bremsstrahlung doses at the i-th layer of IP, respectively, σ_i was the standard error of each measurement, and n was the total number of the IP layers. The chi-squared values from the two spectrometers were combined to find the best-fit parameters in both directions. A contour plot of the chi-squared values for the fitted result for the Cu-CH target is presented in Figure 4(a). The color bar represents the normalized chi-squared value of the corresponding color. The contour map shows a well-defined region in the range of 52° ± 8° and 1.6 ± 0.2 J for a T_h of 1.15 MeV, estimated from an area of two times the minimum chi-squared value in Fig. 4(a). In Figs. 4(b) and 4(c), the simulated doses using the best-fit parameter are compared with the experimental doses. The result shows a good agreement for Brems1, but a slight deviation for Brems2. On investigating the dependence of the slope temperature on the fitting, better agreement between the experiment and the simulation with a lower T_h than that

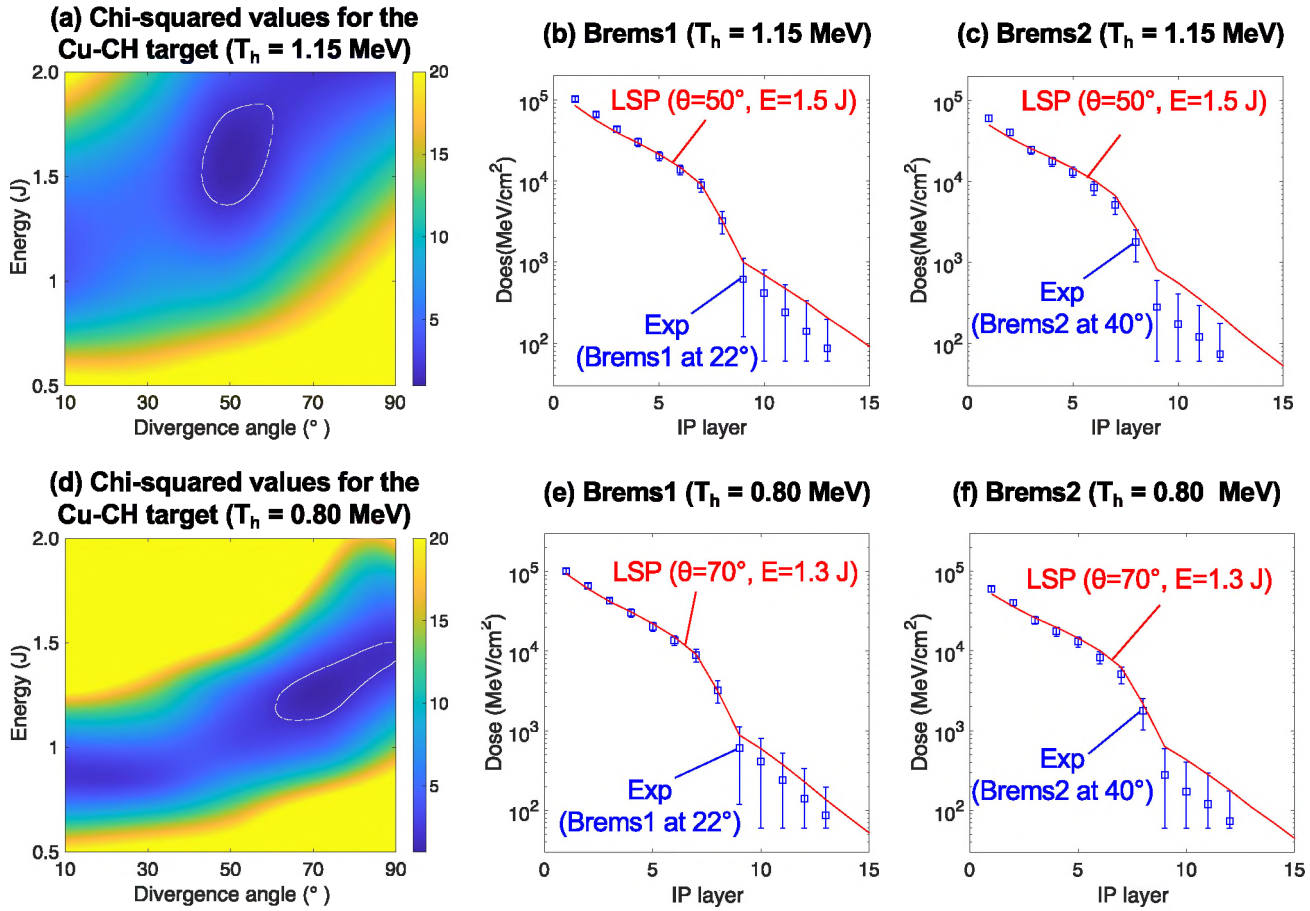

FIG. 4. (a) Contour map of chi-squared values of the fitting result for the Cu-CH target. The contour is a combined result for the fits to the data for both spectrometers. The white dotted lines indicate twice the minimum value in the range of θ=52° ± 8° and E_b=1.6 ± 0.2 J. The color bar shows the chi-squared values. The measurements are compared with a simulation using the best-fit parameter (θ=50°, E_b=1.5 J, T_h=1.15 MeV) for (b) Brems1 and (c) Brems2. (d) Contour map of chi-squared values for T_h=0.80 MeV. The dotted line indicates the range of θ=75° ± 15° and E_b=1.3 ± 0.2 J. (e, f) Comparisons of the experiment with a simulation using θ=70° and E_b=1.3 J at the 22° and 40° positions.

from the measured electron spectrum was found. In Figures 4(d) and 4(f), a contour map of the chi-squared values for a T_h of 0.8 MeV is shown including comparisons of the measured and simulated doses using θ = 70°, and E_b = 1.3 J. The range of θ and E_b inferred from the contour map is estimated to be 75° ± 15° and 1.3 ± 0.2 J. This result indicates that the slope of the electron energy distribution in the laser-interaction region may be lower than that of the escaped electron spectrum. Therefore, the slope temperature of the measured electron spectrum can be a good starting guide for the fitting, but an additional parameter study based on varying the energy spectrum is necessary to find a unique set of the fast electron parameters. In this work, all three electron characteristics have been determined by comparing the fitted results for both the Cu-CH and Cu targets as shown in the next section.

The divergence angle inferred in this study is significantly larger than that found in previous work using 2-D LSP simulations (θ=15° ± 8°).[35] The LSP code in a 2-D Cartesian geometry can appropriately incorporate the electron injection axis and the electron recirculation in simulations, but the transport of fast electrons is solved only in a two-dimensional plane and the absolute photon yields cannot be calculated due to an open system being used. Thus, simulated doses from the 2-D simulations were compared with those from the experiment using arbitrary units. Different divergence angles inferred from the present 3-D and previous 2-D LSP simulations suggested that modeling of the electron recirculation must be performed in a 3-D space. The results that produce a larger divergence angle using a 3-D rather than a 2-D simulation are consistent with the results of implicit 2-D and 3-D PIC simulations.[58]

The conversion efficiency from the laser to fast electrons in a single-slope temperature spectrum was estimated to be 8~10% for this particular shot, with a laser energy of 14.8 J. This value is a lower bound because the electron energy distribution is assumed to be the single slope of the electron spectrum. It is well known that the energy distribution of fast electrons generated in the laser interaction region is described by a continuous spectrum of electrons that can be represented as a sum of multiple exponential slopes. Low-

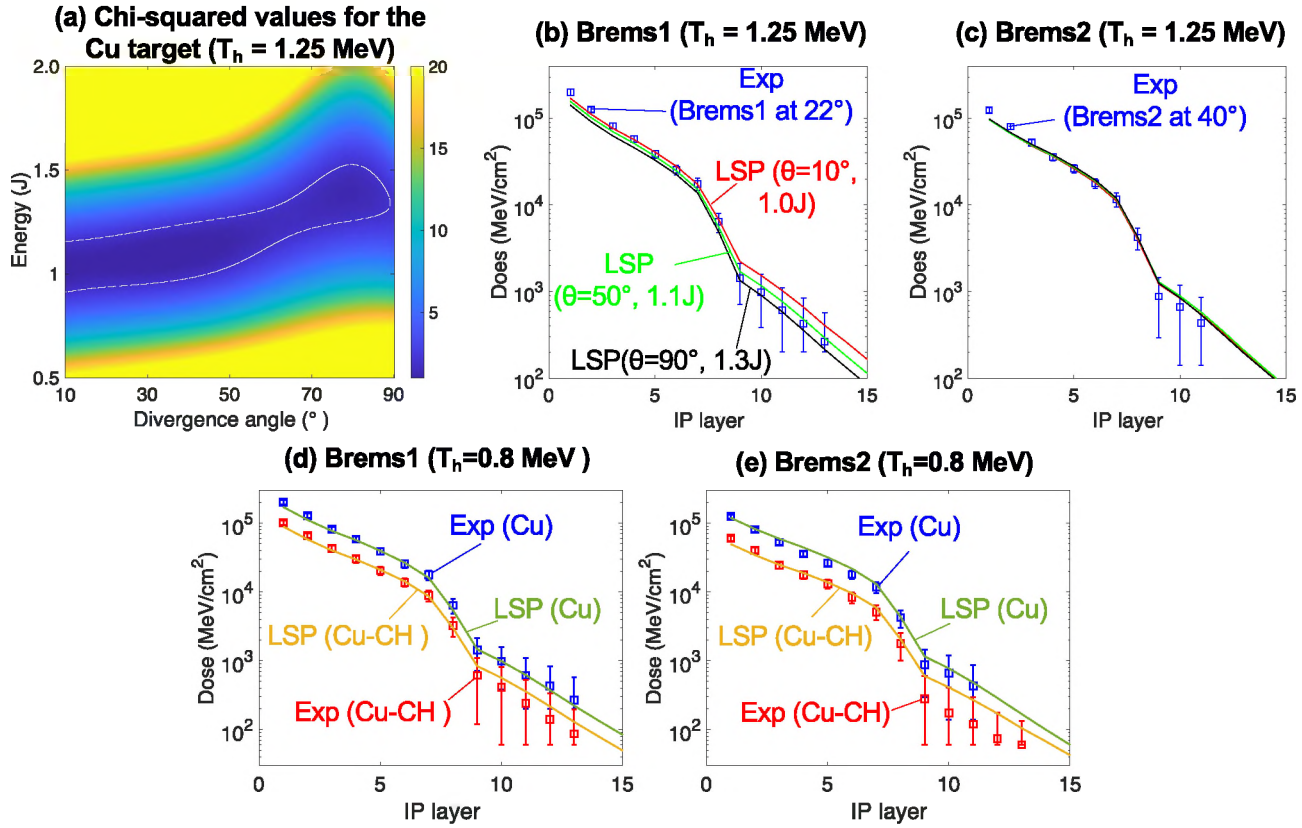

FIG. 5. (a) Chi-squared map of the fitting result using a T_h of 1.25 MeV for the Cu target. Comparisons of the experimental results with the simulated doses for different divergence angles and beam energies for (b) Brems1 and (c) Brems2. Simulations using the same input parameters (θ=70°, E_b=1.3J, T_h=0.80 MeV) for the Cu and Cu-CH targets are compared with the measurements for (d) Brems1 and (e) Brems2.

energy electrons (< tens of keV) contribute less to producing the bremsstrahlung radiation so that the bremsstrahlung measurements would be ineffective in realizing a low energy component. Given that these electrons are trapped by strong magnetic fields in a preplasma or collisionally stopped near the target surface, diagnosing the low-energy component of the spectrum requires alternative measurement techniques. Inclusion of the other electron energy components in the single-slope spectrum would increase the total electron beam energy and conversion efficiency.

B. Fitting to the bremsstrahlung measurements for the Cu target

Fitting of the parameters to the measured bremsstrahlung, similar to that for the Cu-CH target in the previous section, was performed for the strongly refluxing Cu target. An experimental slope temperature of 1.25 MeV, as shown in Fig. 1(b), was chosen for the fitting. A contour plot for the chi-squared values for the fitting results for the Cu target is presented in Figure 5(a). A narrow region of low chi-squared values was found in the electron beam energy across a range of divergence angles, from 10° to 90°. A comparison of the experimental results for three simulated spectrometer doses of θ=10°, 50°, and 90°, respectively, is presented in Figures 5(b) and 5(c). The variation in the input divergence angle did not change the simulated doses, particularly for Brems2, as is clear in Fig. 5(c). The simulation result indicated that the initial divergence angle of an injected electron beam cannot be retrieved from the modeling of the angularly resolved sub-MeV bremsstrahlung radiation from a strongly refluxing target.

However, fast electron characteristics can be deduced by combining the fitting results for both the Cu-CH and Cu targets. It is reasonable to presume that fast electrons with similar characteristics are generated on the surface of the Cu foil in both targets. This assumption allows us to find the overlapping parameter space in Figures 4(a), 4(d), and Figure 5(a). The divergence angle and the beam energy estimated for the Cu-CH target with a T_h of 0.80 MeV (75° ± 15° and 1.3 ± 0.2J) are consistent with the results for the Cu, whereas no common parameter area was found in the case of T_h = 1.15 or 1.25 MeV. Comparisons of the measurements with simulations for a T_h of 0.80 MeV are presented in Figures 5(d) and 5(e). The simulations reproduce well the differences in the bremsstrahlung doses between the Cu and the Cu-CH at both detector positions. The results reveal that

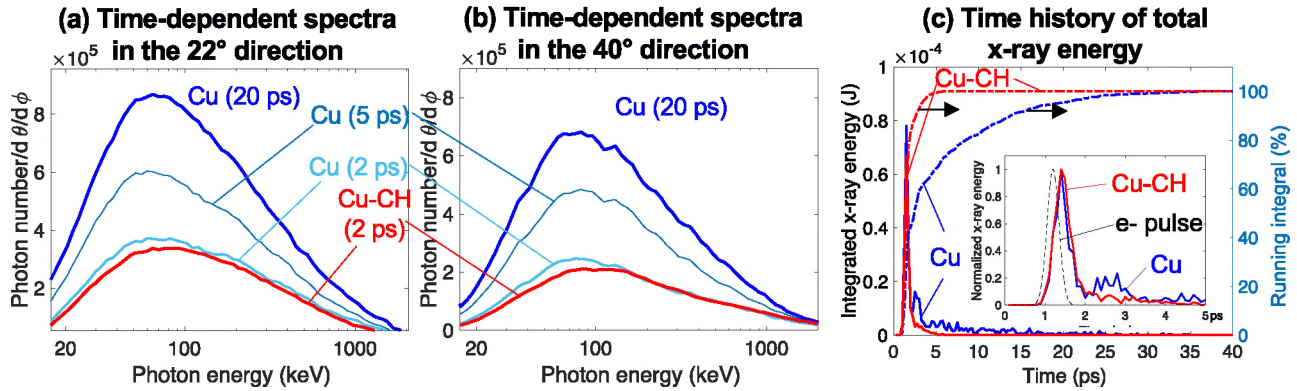

FIG. 6. (a) Temporal evolution of calculated bremsstrahlung spectra between 10 and 2000 keV at the 22° position and (b) at 40° position. (c) A time history of spectrally integrated x-ray energy between 70 and 200 keV along the 22° direction for the Cu and Cu-CH targets. Dotted lines represent running integrals of the x-ray energies as a percentage. The inset in (c) shows the normalized time history for up to 5ps with the 0.35 ps electron pulse peaked at 1.2 ps. The FWHM of the x-ray pulses are 0.39 ps and 0.48 ps for the Cu and Cu-CH targets, respectively.

measurements of the angularly resolved bremsstrahlung signals and escaped electrons from a metallic x-ray source target with and without a large low-Z layer constitute a benchmark data set that can be used to test electron recirculation physics in numerical modeling.

V. Numerical studies of a bremsstrahlung source for hard x-ray radiography

A. Calculations of time-dependent bremsstrahlung radiation between refluxing and non-refluxing targets

The benchmarked LSP code can provide insight into the time-dependent generation of bremsstrahlung radiation of which such measurements are currently unavailable. Two simulations for refluxing and non-refluxing targets were performed with and without a plastic layer using a slope temperature of 0.8 MeV, a divergence angle of 50°, and a beam energy of 1.3J, respectively. The simulation for the Cu target was run for up to 40 ps. The temporal evolutions of the bremsstrahlung spectra between 10 and 2000 keV at the 22° and 40° detector positions are presented in Figures 6(a) and 6(b). The spectral intensities were comparable up to ~2 ps. After 2 ps, the x-ray spectra from the Cu becomes more intense by a factor of ~2.2 (~3.3) at 22° (40°) around 100 keV at 20 ps compared to those for the Cu-CH target [differences between the red (2 ps) and blue (20 ps) curves in Fig.6(a) and 6(b)]. The phenomenon of an enhancement in the x-ray yields due to electron recirculation is well known. Here, the simulation shows, for the first time, that the bremsstrahlung spectrum peaking at ~ 70 keV continues to increase with time.

To examine the duration of the x-ray emission, the bremsstrahlung spectrum was integrated with respect to the photon energy between 70 keV and 200 keV, and whose spectral range is an effective backlighter spectrum for broadband x-ray radiography (Compton radiography) of an ICF implosion core.[59,60] The time histories of the integrated x-ray energy for the Cu and Cu-CH targets in the 22° detector direction are given in Figure 6(c). The inset in the figure shows the time between 0 and 5 ps along with the electron pulse history. The rising edge of the x-ray generation and the time of the x-ray peak are almost identical for both targets. These traces start to diverge from one another after the x-ray production reaches a peak around 1.5 ps, which is slightly later than the peak of the electron pulse at 1.2 ps. [see black dotted line in the inset of Fig.6(c)]. The x-ray intensity of the Cu-CH target rapidly decays as the electron beam exits from the Cu foil at around 2.5 ps, and becomes zero at ~5 ps. In contrast, electron recirculation in the Cu foil produces weak x-ray emission for ~ 25 ps. In Fig.6(c), running integrals of the x-ray energy history are calculated and plotted as dotted lines. These plots reveal that 95% of the x-ray energy between 70 and 200 keV is produced within 3 ps for the Cu-CH target, while reaching 95% for the Cu target takes ~25 ps, although 50% of the x-ray energy is produced in ~ 3 ps. It is important to note that the duration of the x-ray emission presented here is an upper limit because (1) the simulations exclude a proton layer on the rear side of the target that weakens the magnitude of the sheath potentials when they are accelerated via Target Normal Sheath Acceleration, reducing the number of recirculated electrons, and (2) the thermal expansion of the target due to heating is neglected. Nonetheless, this result indicates that care must be taken when a rapidly evolving object such as a laser-driven implosion core is radiographed with a laser-driven x-ray source using an isolated solid target. Such a long-lasting x-ray emission due to electron recirculation has been measured in a radiography experiment at the National Ignition Facility (NIF). An x-ray streak measurement has shown that a spectrally integrated x-ray emission persists over ~300 ps when a 30 ps NIF ARC beam irradiates an Au wire target.[60] 3-D hybrid PIC modeling of time-dependent sub-ps laser-produced bremsstrahlung could be extended to simulate the electron transport and bremsstrahlung generated by multi-ps short-pulse lasers.

B. Mitigation of electron recirculation using various volumes of plastic backing

Suppression of electron recirculation and hard x-ray generation was studied numerically by varying the volume of the plastic backing. Finding the minimum volume of plastic necessary to eliminate the effects of electron recirculation is conducive to obtaining simulation box sizes and designing refluxing-controlled targets for experiments. Within our simulation box size ($2\times1.5\times2$ mm^3), the thickness and surface area of the CH backing were varied from 100 μm to 650 μm, and from 1 mm^2 to 2 mm^2, respectively. The largest volume of the CH that fits the simulation box was 650 μm in thickness and 2 mm^2 in surface area. A CH backing reaching the absorbing boundaries was treated as infinitely long. These simulations were performed using T_h = 0.8 MeV, θ = 50°, and E_b = 1.3J. The spectra of the space-integrated hard x-ray photons generated in a 100-μm-thick Cu foil with different volumes of CH backing are presented in Figure 7. Self-x-ray attenuation by the targets was not taken into account and calculated for the spectra. The addition of a CH backing to the Cu reduces the photon spectrum uniformly over a broad photon energy range up to ~ 1 MeV. Attaching a 500-μm-thick CH with a 1 mm^2 surface area to the Cu decreases the spectral intensity by a factor of ~2, but this reduction is not large enough to eliminate electrons recirculating back to the Cu. A photon spectrum for an infinitely large CH slab is reproduced for a 500-μm-thick CH slab with an infinite surface area (2 mm^2) and a 1mm2 surface area with an infinitely long thickness (not shown in Fig.7). This indicates that the effects of electron recirculation can be suppressed with at least a 500 μm thick plastic layer and a large surface area (> 2 mm^2) for a T_h of 0.8 MeV. It is noted that the minimum volume of plastic required for diminishing the effects of electron recirculation would change with a peak laser intensity generating an electron energy distribution.

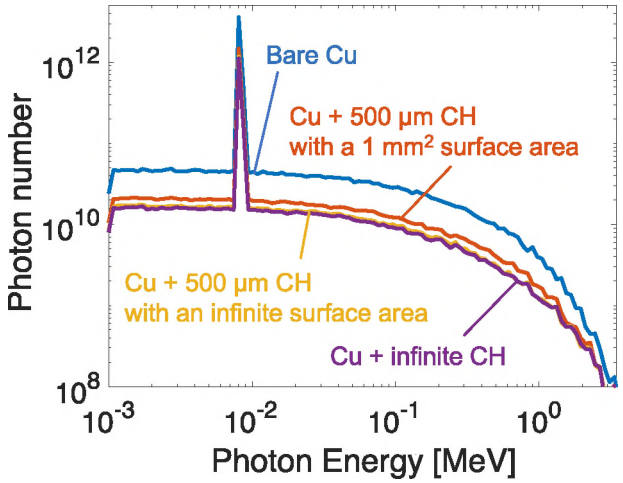

FIG.7 Simulated hard x-ray spectra from a 100 μm thick Cu foil with various different CH backing volumes (no backing, 500 μm thick × 1 mm^2, 500 μm × 2 mm^2, and 650 μm × 2 mm^2 backings).

VI. CONCLUSIONS

We have characterized sub-ps laser-produced fast electrons by modeling angularly resolved bremsstrahlung measurements for the refluxing and non-refluxing targets with the 3-D hybrid PIC LSP code. The bremsstrahlung and escaped electron measurements were made for the strongly refluxing 100-μm-thick Cu foil and a non-refluxing Cu foil with a large CH layer. The divergence angle and conversion efficiency were determined from simultaneous fitting of the two bremsstrahlung signals with simulations, while a slope temperature of the electron energy spectrum was estimated from the electron measurement. It was found that all three electron parameters could not be determined uniquely from either fitting to the Cu-CH or the Cu data. Assuming the same electron source was generated in both targets, agreements between the simulation and experiment were found for both datasets using the divergence angle and beam energy (conversion efficiency) of 70° and 1.3 J (8.9 %), respectively, for a slope temperature of 0.8 MeV. The results demonstrate that angularly resolved bremsstrahlung measurements from a metal foil with and without a large low-Z layer to control electron recirculation can provide benchmarking data for a 3-D hybrid PIC code. Future work will include studies of electron recirculation with different laser conditions (laser energy, pulse duration, and peak intensity).

The 3-D LSP simulations provided new insights into the time evolution of angular-dependent bremsstrahlung radiation. The enhancement of x-ray photons generated in the Cu was uniform over a broad-spectrum range between 10 keV and 1 MeV. The time history of the integrated x-ray photon energy between 70 and 200 keV, and the range relevant for radiographs of an ICF implosion core, showed that the x-rays from an isolated Cu foil were emitted for a period 8~10 times longer than that from a Cu foil with a CH backing. This could cause blurring in a radiographic image of a rapidly evolving object (e.g., implosion core). The benchmarked 3-D hybrid PIC code could be used to predict fast-electron-induced, hard-x-ray sources for applications in radiography.

ACKNOWLEDGEMENTS

The authors would like to acknowledge Drs. T. S. Daykin, F. N. Beg, H. Chen, A. J. Link, G. J. Williams, Y. Ping, and H. S. McLean for their support in obtaining the experimental data. This work was supported by the National Science Foundation under Grant No. 1707357 through the NSF/DOE Partnership in Basic Plasma Science and Engineering. This material is based upon work supported by the U.S. Department of Energy, Office of Science, Office of Fusion Energy Sciences, High Energy Density Laboratory Plasmas program under Award Number DE-SC0022236.

AUTHOR DECLARATIONS

Conflict of Interest

The authors have no conflicts of interest to disclose.

DATA AVAILABILITY

The data that support the findings of this study are available from the corresponding author upon reasonable request.

[1] M.D. Perry, J.A. Sefcik, T. Cowan, S. Hatchett, A. Hunt, M. Moran, D. Pennington, R. Snavely, and S.C. Wilks, Rev. Sci. Instrum. 70, 265 (1999).
[2] M. Schnürer, M.P. Kalashnikov, P. V. Nickles, T. Schlegel, W. Sandner, N. Demchenko, R. Nolte, and P. Ambrosi, Phys. Plasmas 2, 3106 (1995).
[3] H. Sawada, C.M. Salinas, F.N. Beg, H. Chen, A.J. Link, H.S. McLean, P.K. Patel, Y. Ping, J. Williams, and G.J. Williams, Plasma Phys. Control. Fusion 62, 065001 (2020).
[4] K. Li, B. Borm, F. Hug, D. Khaghani, B. Loher, D. Savran, N. A. Tahir, and P. Neumayer, Laser Part. Beams 32, 631 (2014).
[5] R. Tommasini, H.S. Park, P. Patel, B. Maddox, S. Le Pape, S.P. Hatchett, B.A. Remington, M.H. Key, N. Izumi, M. Tabak, J.A. Koch, O.L. Landen, D. Hey, A. MacKinnon, J. Seely, G. Holland, L. Hudson, and C. Szabo, AIP Conf. Proc. **926**, 248 (2007).
[6] R. Tommasini, S.P. Hatchett, D.S. Hey, C. Iglesias, N. Izumi, J. A. Koch, O.L. Landen, A. J. MacKinnon, C. Sorce, J. A. Delettrez, V.Y. Glebov, T.C. Sangster, and C. Stoeckl, Phys. Plasmas 18, 056309 (2011).
[7] R. Tommasini, O.L. Landen, L.B. Hopkins, S.P. Hatchett, D.H. Kalantar, W.W. Hsing, D.A. Alessi, S.L. Ayers, S.D. Bhandarkar, M.W. Bowers, D.K. Bradley, A.D. Conder, J.M. Di Nicola, P. Di Nicola, L. Divol, D. Fittinghoff, G. Gururangan, G.N. Hall, M. Hamamoto, D.R. Hargrove, E.P. Hartouni, J.E. Heebner, S.I. Herriot, M.R. Hermann, J.P. Holder, D.M. Holunga, D. Homoelle, C.A. Iglesias, N. Izumi, A.J. Kemp, T. Kohut, J.J. Kroll, K. Lafortune, J.K. Lawson, R. Lowe-Webb, A.J. Mackinnon, D. Martinez, N.D. Masters, M.P. Mauldin, J. Milovich, A. Nikroo, J.K. Okui, J. Park, M. Prantil, L.J. Pelz, M. Schoff, R. Sigurdsson, P.L. Volegov, S. Vonhof, T.L. Zobrist, R.J. Wallace, C.F. Walters, P. Wegner, C. Widmayer, W.H. Williams, K. Youngblood, M.J. Edwards, and M.C. Herrmann, Phys. Rev. Lett. 125, 1155003 (2020).
[8] M. Tabak, J. Hammer, M.E. Glinsky, W.L. Kruer, S.C. Wilks, J. Woodworth, E.M. Campbell, M.D. Perry, and R.J. Mason, Phys. Plasmas 1, 1626 (1994).
[9] R. Kodama, P. A. Norreys, K. Mima, A. E. Dangor, R.G. Evans, H. Fujita, Y. Kitagawa, K. Krushelnick, T. Miyakoshi, N. Miyanaga, T. Norimatsu, S.J. Rose, T. Shozaki, K. Shigemori, A. Sunahara, M. Tampo, K. A. Tanaka, Y. Toyama, T. Yamanaka, and M. Zepf, Nature 412, 798 (2001).
[10] A. Schönlein, G. Boutoux, S. Pikuz, L. Antonelli, D. Batani, A. Debayle, A. Franz, L. Giuffrida, J.J. Honrubia, J. Jacoby, D. Khaghani, P. Neumayer, O.N. Rosmej, T. Sakaki, J.J. Santos, and A. Sauteray, Epl **114**, (2016).
[11] H. Schwoerer, P. Gibbon, S. Düsterer, R. Behrens, C. Ziener, C. Reich, and R. Sauerbrey, Phys. Rev. Lett. 86, 2317 (2001).
[12] C. Courtois, R. Edwards, A. Compant La Fontaine, C. Aedy, S. Bazzoli, J.L. Bourgade, J. Gazave, J.M. Lagrange, O. Landoas, L. Le Dain, D. Mastrosimone, N. Pichoff, G. Pien, and C. Stoeckl, Phys. Plasmas 20, 083114 (2013).
[13] S. Li, B. Shen, J. Xu, T. Xu, Y. Yu, J. Li, X. Lu, C. Wang, X. Wang, X. Liang, Y. Leng, R. Li, and Z. Xu, Phys. Plasmas 24, 093104 (2017).
[14] K.B. Wharton, S.P. Hatchett, S.C. Wilks, M.H. Key, J.D. Moody, V. Yanovsky, A.A. Offenberger, B.A. Hammel, M.D. Perry, and C. Joshi, Phys. Rev. Lett. 81, 822 (1998).
[15] A.P.L. Robinson, D.J. Strozzi, J.R. Davies, L. Gremillet, J.J. Honrubia, T. Johzaki, R.J. Kingham, M. Sherlock, and A.A. Solodov, Nucl. Fusion **54**, (2014).
[16] M.H. Key, M.D. Cable, T.E. Cowan, K.G. Estabrook, B.A. Hammel, S.P. Hatchett, E.A. Henry, D.E. Hinkel, J.D. Kilkenny, J.A. Koch, W.L. Kruer, A.B. Langdon, B.F. Lasinski, R.W. Lee, B.J. MacGowan, A. MacKinnon, J.D. Moody, M.J. Moran, A.A. Offenberger, D.M. Pennington, M.D. Perry, T.J. Phillips, T.C. Sangster, M.S. Singh, M.A. Stoyer, M. Tabak, G.L. Tietbohl, M. Tsukamoto, K. Wharton, and S.C. Wilks, Phys. Plasmas 5, 1966 (1998).
[17] A.G. MacPhee, K.U. Akli, F.N. Beg, C.D. Chen, H. Chen, R. Clarke, D.S. Hey, R.R. Freeman, A.J. Kemp, M.H. Key, J.A. King, S. Le Pape, A. Link, T.Y. Ma, H. Nakamura, D.T. Offermann, V.M. Ovchinnikov, P.K. Patel, T.W. Phillips, R.B. Stephens, R. Town, Y.Y. Tsui, M.S. Wei, L.D. Van Woerkom, and A.J. MacKinnon, Rev. Sci. Instrum. 79, 10F302 (2008).
[18] P. Norreys, D. Batani, S. Baton, F.N. Beg, R. Kodama, P.M. Nilson, P. Patel, F. Pérez, J.J. Santos, R.H.H. Scott, V.T. Tikhonchuk, M. Wei, and J. Zhang, Nucl. Fusion 54, 054004 (2014).
[19] R. Nolte, R. Behrens, M. Schnürer, A. Rousse, and P. Ambrosi, Radiat. Prot. Dosim. 84, 367 (1999).
[20] C.D. Chen, J.A. King, M.H. Key, K.U. Akli, F.N. Beg, H. Chen, R.R. Freeman, A. Link, A.J. MacKinnon, A.G. MacPhee, P.K. Patel, M. Porkolab, R.B. Stephens, and L.D. Van Woerkom, Rev. Sci. Instrum. **79**, 529 (2008).
[21] R.H.H. Scott, F. Pérez, M.J.V. Streeter, E.L. Clark, J.R. Davies, H.P. Schlenvoigt, J.J. Santos, S. Hulin, K.L. Lancaster, F. Dorchies, C. Fourment, B. Vauzour, A.A. Soloviev, S.D. Baton, S.J. Rose, and P.A. Norreys, New J. Phys. **15**, (2013).
[22] D.R. Rusby, C.D. Armstrong, C.M. Brenner, R.J. Clarke, P. McKenna, and D. Neely, Rev. Sci. Instrum. 89, 073502 (2018).
[23] C.D. Chen, P.K. Patel, D.S. Hey, A.J. MacKinnon, M.H. Key, K.U. Akli, T. Bartal, F.N. Beg, S. Chawla, H. Chen, R.R. Freeman, D.P. Higginson, A. Link, T.Y. Ma, A.G. MacPhee, R.B. Stephens, L.D. Van Woerkom, B. Westover, and M. Porkolab, Phys. Plasmas **16**, 1 (2009).
[24] P. Neumayer, B. Aurand, M. Basko, B. Ecker, P. Gibbon, D.C. Hochhaus, a. Karmakar, E. Kazakov, T. Kühl, C. Labaune, O. Rosmej, A. Tauschwitz, B. Zielbauer, and D. Zimmer, Phys. Plasmas 17, 103103 (2010).
[25] B. Westover, C.D. Chen, P.K. Patel, M.H. Key, H. McLean, R. Stephens, and F.N. Beg, Phys. Plasmas **18**, 1 (2011).
[26] H. Sawada, Y. Sentoku, A. Bass, B. Griffin, R. Pandit, F. Beg, H. Chen, H. McLean, A.J. Link, P.K. Patel, and Y. Ping, J. Phys. B At. Mol. Opt. Phys. 48, 224008 (2015).
[27] A. Compant La Fontaine, C. Courtois, F. Gobet, F. Hannachi, J.R. Marquès, M. Tarisien, M. Versteegen, and T. Bonnet, Phys. Plasmas 26, (2019).
[28] C.D. Armstrong, C.M. Brenner, E. Zemaityte, G.G. Scott, D.R. Rusby, G. Liao, H. Liu, Y. Li, Z. Zhang, Y. Zhang, B. Zhu, P. Bradford, N.C. Woolsey, P. Oliveira, C. Spindloe, W. Wang, P. McKenna, and D. Neely, Plasma Phys. Control. Fusion (2019).
[29] M. Li, H. An, G. Hu, J. Xiong, A. Lei, Z. Xie, C. Wang, W. Wang, Z. Zhang, and L. Huang, Phys. Plasmas 29, 013107 (2022).
[30] C.D. Chen, A.J. Kemp, F. Pérez, A. Link, F.N. Beg, S. Chawla, M.H. Key, H. McLean, A. Morace, Y. Ping, A. Sorokovikova, R.B. Stephens, M. Streeter, B. Westover, and P.K. Patel, Phys. Plasmas 20, 052703 (2013).
[31] B. Westover, C.D. Chen, P.K. Patel, H. McLean, and F.N. Beg, Phys. Plasmas 21, 0 (2014).
[32] K. McKeever, M. Makita, G. Nersisyan, T. Dzelzainis, S. White, B. Kettle, B. Dromey, M. Zepf, G. Sarri, D. Doria, H. Ahmed, C.L.S. Lewis, D. Riley, and A.P.L. Robinson, Phys. Rev. E - Stat. Nonlinear, Soft Matter Phys. 91, 033107 (2015).
[33] S. Fujioka, T. Johzaki, Y. Arikawa, Z. Zhang, A. Morace, T. Ikenouchi, T. Ozaki, T. Nagai, Y. Abe, S. Kojima, S. Sakata, H. Inoue, M. Utsugi, S. Hattori, T. Hosoda, S.H. Lee, K. Shigemori, Y. Hironaka, A. Sunahara, H. Sakagami, K. Mima, Y. Fujimoto, K. Yamanoi, T. Norimatsu, S. Tokita, Y. Nakata, J. Kawanaka, T. Jitsuno, N. Miyanaga, M. Nakai, H. Nishimura, and H. Shiraga, Phys. Rev. E 91, 063102 (2015).
[34] J. Peebles, M.S. Wei, A. V. Arefiev, C. McGuffey, R.B. Stephens, W. Theobald, D. Haberberger, L.C. Jarrott, A. Link, H. Chen, H.S. McLean, A. Sorokovikova, S. Krasheninnikov, and F.N. Beg, New J. Phys. 19, 023008 (2017).
[35] T.S. Daykin, H. Sawada, Y. Sentoku, F.N. Beg, H. Chen, H.S. McLean, A.J. Link, P.K. Patel, and Y. Ping, Phys. Plasmas **25**, (2018).
[36] B. Borm, D. Khaghani, and P. Neumayer, Phys. Plasmas 26, 023109 (2019).
[37] A.J. Mackinnon, Y. Sentoku, P.K. Patel, D.W. Price, S. Hatchett, M.H. Key, C. Andersen, R. Snavely, and R.R. Freeman, Phys. Rev. Lett. 88, 215006 (2002).

[38] Y. Sentoku, T.E. Cowan, A. Kemp, and H. Ruhl, Phys. Plasmas 10, 2009 (2003).
[39] Y. Sentoku, K. Mima, P. Kaw, and K. Nishikawa, Phys. Rev. Lett. 90, 4 (2003).
[40] D. Welch, D. Rose, B. Oliver, and R. Clark, Nucl. Instrum. Methods Phys. Res., Sect. A 464, 134 (2001).
[41] E. Martinolli, M. Koenig, F. Amiranoff, S.D. Baton, L. Gremillet, J.J. Santos, T.A. Hall, M. Rabec-Le-Gloahec, C. Rousseaux, and D. Batani, Phys. Rev. E 70, 55402 (2004).
[42] T. Yabuuchi, B.S. Paradkar, M.S. Wei, J.A. King, F.N. Beg, R.B. Stephens, N. Nakanii, M. Hatakeyama, H. Habara, K. Mima, K.A. Tanaka, and J.T. Larsen, Phys. Plasmas 17, 060704 (2010).
[43] M.N. Quinn, X.H. Yuan, X.X. Lin, D.C. Carroll, O. Tresca, R.J. Gray, M. Coury, C. Li, Y.T. Li, C.M. Brenner, a P.L. Robinson, D. Neely, B. Zielbauer, B. Aurand, J. Fils, T. Kuehl, and P. McKenna, Plasma Phys. Control. Fusion 53, 025007 (2011).
[44] P.P. Wiewior, A. Astanovitskiy, G. Aubry, S. Batie, J. Caron, O. Chalyy, T. Cowan, C. Haefner, B. Galloudec, N. Galloudec, D. Macaulay, V. Nalajala, G. Pettee, S. Samek, Y. Stepanenko, and J. Vesco, J. Fusion Energy 28, 218 (2008).
[45] H. Sawada, Y. Sentoku, T. Yabuuchi, U. Zastrau, E. Förster, F.N. Beg, H. Chen, A.J. Kemp, H.S. McLean, P.K. Patel, and Y. Ping, Phys. Rev. Lett. 122, 155002 (2019).
[46] H. Chen, A.J. Link, R. Van Maren, P.K. Patel, R. Shepherd, S.C. Wilks, and P. Beiersdorfer, Rev. Sci. Instrum. **79**, 8 (2008).
[47] A. Link, R.R. Freeman, D.W. Schumacher, and L.D. Van Woerkom, Phys. Plasmas 18, 053107 (2011).
[48] D.R. Rusby, C.D. Armstrong, G.G. Scott, M. King, P. McKenna, and D. Neely, High Power Laser Sci. Eng. (2019).
[49] M. Roth and M. Schollmeier, Cern Yellow Reports 1, 231 (2016).
[50] P. Mora, Phys. Rev. Lett. 90, 185002 (2003)
[51] M. Li, H. An, G. Hu, J. Xiong, A. Lei, Z. Xie, C. Wang, W. Wang, Z. Zhang, and L. Huang, Phys. Plasmas 29, 013107 (2022).
[52] S. Atzeni, A Schiavi, and J.R. Davies, Plasma Phys. Control. Fusion 51, 015016 (2009)
[53] D. Groom and S. Klein, The European Physical Journal C-Particles and Fields 15, 163–173 (2000)
[54] S.M. Seltzer and M.J. Berger, IEEE Trans. Nucl. Sci. **39**, 1025 (1992).
[55] H. Hirayama, Y. Namito, A. F. Bielajew, S. J. Wilderman, and W. R. Nelson, "The EGS5 code system," SLAC-R-730 and KEK Report 2005- 8 (SLAC National Accelerator Laboratory and High Energy Accelerator Research Organization, Menlo Park, USA and Tsukuba, Japan, 2005).
[56] T. Sato, Y. Iwamoto, S. Hashimoto, T. Ogawa, T. Furuta, S. ichiro Abe, T. Kai, P.E. Tsai, N. Matsuda, H. Iwase, N. Shigyo, L. Sihver, and K. Niita, J. Nucl. Sci. Technol. **55**, 684 (2018).
[57] H. Sawada, T.S. Daykin, T.M. Hutchinson, B.S. Bauer, V. V. Ivanov, F.N. Beg, H. Chen, G.J. Williams, and H.S. McLean, Phys. Plasmas 26, 083104 (2019).
[58] K.D. Xiao, C.T. Zhou, K. Jiang, Y.C. Yang, R. Li, H. Zhang, B. Qiao, T.W. Huang, J.M. Cao, T.X. Cai, M.Y. Yu, S.C. Ruan, and X.T. He, Phys. Plasmas **25**, 023103 (2018).
[59] R. Tommasini, A. MacPhee, D. Hey, T. Ma, C. Chen, N. Izumi, W. Unites, A. MacKinnon, S.P. Hatchett, B. a Remington, H.S. Park, P. Springer, J. a Koch, O.L. Landen, J. Seely, G. Holland, and L. Hudson, Rev. Sci. Instrum. 79, 10E901 (2008).
[60] R. Tommasini, C. Bailey, D.K. Bradley, M. Bowers, H. Chen, J.M. Di Nicola, P. Di Nicola, G. Gururangan, G.N. Hall, C.M. Hardy, D. Hargrove, M. Hermann, M. Hohenberger, J.P. Holder, W. Hsing, N. Izumi, D. Kalantar, S. Khan, J. Kroll, O.L. Landen, J. Lawson, D. Martinez, N. Masters, J.R. Nafziger, S.R. Nagel, A. Nikroo, J. Okui, D. Palmer, R. Sigurdsson, S. Vonhof, R.J. Wallace, and T. Zobrist, Phys. Plasmas 24, 053104 (2017).